Impact of Ser17 Phosphorylation on the Conformational Dynamics of the Oncoprotein MDM2

Impact of Ser17 phosphorylation on the conformational dynamics of the oncoprotein MDM2

Juan A. Bueren-Calabuig[1,2] *and Julien Michel*[1*]

[1] EaStCHEM School of Chemistry, the University of Edinburgh, Edinburgh, EH9 3FJ, UK
[2] Computational Biology, School of Life Sciences. School of Science and Engineering, University of Dundee, Dow Street, Dundee, DD1 5EH, UK

Corresponding Author:

Dr. Julien Michel,
School of Chemistry
Joseph Black Building, University of Edinburgh
David Brewster Road
Edinburgh
EH9 3FJ
United Kingdom
phone: +44 (0)131 650 4797
E-mail: mail@julienmichel.net

Funding

JM is supported by a Royal Society University Research Fellowship. This research was funded by the Engineering and Physical Sciences Research Council (EPSRC), grant number EP/K002082/1. This project made use of time on ARCHER granted via the UK High-End Computing Consortium for Biomolecular Simulation, HECBioSim (http://hecbiosim.ac.uk), supported by EPSRC (grant no. EP/L000253/1)

Abbreviations:

MDM2, murine double minute 2; TAD, transactivation domain; pS17, phosphorylated Ser17; MD, molecular dynamics; cMD, conventional molecular dynamics; aMD, accelerated molecular dynamis; US, umbrella sampling; vFEP, variational free energy profile; WT-MDM2, wild-type MDM2; CV, collective variable

Abstract

MDM2 is an important oncoprotein that downregulates the activity of the tumour suppressor protein p53 via binding of its N-terminal domain to the p53 transactivation domain. The first 24 residues of the MDM2 N-terminal domain form an intrinsically disordered “lid” region that interconverts on millisecond time scale between “open” and “closed” states in unliganded MDM2. While the former conformational state is expected to facilitate p53 binding, the latter competes in a pseudo-substrate manner with p53 for its binding site. Phosphorylation of serine 17 in the MDM2 lid region is thought to modulate the equilibrium between “open” and “closed” lid states, but contradictory findings on the favoured lid conformational state upon phosphorylation have been reported. Here the nature of the conformational states of MDM2 pSer17 and Ser17Asp variants was addressed by means of enhanced sampling molecular dynamics simulations. Detailed analyses of the computed lid conformational ensembles indicate that both lid variants stabilise a “closed” state with respect to wild type. Nevertheless the nature of the closed state conformational ensembles differs significantly between the pSer17 and Ser17Asp variants. Thus care should be applied in the interpretation of biochemical experiments that use phospho-mimetic variants to model the effects of phosphorylation on the structure and dynamics of this disordered protein region.

The tumor suppressor protein p53 is down-regulated by the ubiquitin ligase MDM2 in normal cells. This negative control occurs via recognition of the trans-activation domain (TAD) of p53 by the N-terminal region of MDM2 (ca.120 residues), which in turn initiates ubiquitination and degradation of p53.[1-4] However, in response to stress conditions in the cell (e.g. DNA damage), phosphorylation of MDM2 and/or p53 can lead to p53 activation by disruption of p53/MDM2 complexes.[5-9] In more than 50% of tumors, this regulatory mechanism is altered as a result of MDM2 overexpression, leading to inactivation of the tumor-supressive functions of p53 such as apoptosis or cell repair.[10,11]

Despite important efforts to elucidate the role played by phosphorylations in p53 reactivation by MDM2,[12] detailed molecular mechanisms remain elusive. Attention has focussed especially on phosphorylation of MDM2 residue Ser17 that is located within a disordered, flexible "lid" (residues 1-24) region of the N-terminal domain of MDM2. The remainder of the domain, residues 25-120, is natively folded and referred as the MDM2 "core" region in this report. The MDM2 core region contains the p53 binding site within the "Phe19-Trp23-Leu26 hydrophobic cleft" (Figure 1). In unliganded MDM2 the lid region is in equilibrium between a "closed" state that competes with p53 for access to the p53 binding site via a pseudo-substrate mechanism, and an "open" state in which the lid is distant from the p53 binding site, enabling access to p53.[13] Diverse approaches including biochemical, biophysical and computer modelling have sought insights into the molecular mechanisms by which phosphorylation of Ser17 modulates MDM2 interactions with p53.[13-17] McCoy et al. performed NMR measurements on a Ser17Asp (S17D) phospho-mimetic MDM2 construct (16-125) to conclude that Ser17 phosphorylation increased the affinity of the lid for the MDM2 hydrophobic pocket, and hindered formation of p53-MDM2 complex.[13] By contrast, Worrall et al. showed via

biochemical studies an increase of the ubiquitin ligase activity of full-length phospho-mimetic MDM2, which they attributed to an enhanced stability of MDM2-p53 complexes due to stabilisation of the phosphorylated lid in an open state.[14,16,17] In disagreement with these results Zhan et al.,[15] reported biochemical experiments suggesting that neither phosphorylation of Ser17 nor Ser17Asp mutation have a significant effect on the binding of p53 TAD to MDM2.

Molecular dynamics simulations studies have sought to establish how phosphorylated pSer17 or Ser17Asp modifications modulate the conformational preferences of the MDM2 lid.[18-20] Conventional protein MD simulations sample readily nano to micro second timescales of dynamics, which is insufficient for studies of the MDM2 lid dynamics since NMR experiments have shown that the MDM2 lid exchanges between "closed" and "open" conformations on a ca. 10 ms time scale.[21] To facilitate MD studies of disordered protein regions,[22] our group has proposed and applied different computational methodologies to c-Myc,[23] and MDM2.[24] The methodology used for the preceding MDM2 study of apo and holo wild type lid dynamics combined accelerated molecular dynamics (aMD),[25-27] umbrella sampling (US)[28] and variational free energy profile (vFEP)[29,30] techniques. Given the experimental uncertainties in the impact of MDM2 phosphorylation on lid interactions, this protocol was here applied to establish the conformational preferences of unliganded wild type, pSer17 and Ser17Asp MDM2 lid variants.

Materials and Methods

Detailed description of system setup and MD simulation protocols is fully described in previous work on holo MDM2 lid dynamics.[24] For the sake of clarity the protocol is briefly described below and emphasis is given on methodological aspects specific to the present work.

Systems setup

Three different models of the N-terminal domain of human MDM2 were prepared for molecular modelling studies: wild-type MDM2 (WT-MDM2), phosphorylated Ser17 MDM2 (pSer17-MDM2), and the phospho-mimetic Asp17 variant (S17D-MDM2). All models were based on the NMR solution ensemble of the N-terminal domain of MDM2 (residues 1-119) (PDB ID:1Z1M).[31] Models were prepared with the leap utility from the Amber12 suite,[32] using the ff99SBildnmr forcefield.[33] Forcefield parameters for phosphorylated Ser17 were taken from Homeyer et al.[34] Each protein was immersed in a cubic periodic box of TIP3P water molecules[35] that extended 15Å away from any solute atom and neutralized by addition of appropriate number of Cl^- counter ions.[36]

Molecular dynamics simulations protocols

The MDM2 lid region interchanges between closed and open conformation on a multi ms time-scale.[21] As a result, conventional molecular dynamics (cMD) protocols are insufficient to efficiently sample the thermally accessible conformational space of the MDM2 lid region. This limitation was here overcome by combining accelerated molecular dynamics (aMD),[25-27] umbrella sampling (US)[28] and variational free energy profile (vFEP) methodologies.[29,30] Preliminary cMD simulations were performed to determine the parameters needed to set up aMD simulations. Unlike methodologies such as metadynamics,[37,38] aMD does not require a predefined collective variable to enhance the sampling. In aMD a biasing term, $\Delta V(\mathbf{r})$, is added when the the potential energy function, $V(\mathbf{r})$, is below a predefined value (E_p). The resulting potential, $V^*(\mathbf{r})$, given by Eq1, contributes to reducing the height of energy barriers that separates different energy minima:

$$V^*(\boldsymbol{r}) = \begin{cases} V(\boldsymbol{r}) & V(\boldsymbol{r}) > E_p \\ V(\boldsymbol{r}) + \Delta V(\boldsymbol{r}) & V(\boldsymbol{r}) < E_p \end{cases}. \quad (1)$$

In this work, 100ns aMD simulations were run for each system, using a dual boost protocol: one boost was applied to the total potential energy and an extra boost was added to the dihedral torsions (using iamd=3 keyword in AMBER 12):

$$\Delta V(\boldsymbol{r}) = \frac{(E_P - V(\boldsymbol{r}))^2}{(\alpha_p + E_p - V(\boldsymbol{r}))} + \frac{(E_D - V_D(\boldsymbol{r}))^2}{(\alpha_D + E_D - V_D(\boldsymbol{r}))}, \quad (2)$$

where V_D is the dihedral energy, E_P and E_D are the reference potential and dihedral energies and αP and αD are the acceleration parameters that describe the strength of the boost for each term. The chosen aMD parameters were initially set according to guidelines from previous works, [25,39] and subsequently modified until an enhancement in the sampling of lid conformations was achieved. The final parameters are shown in Table S1. To further focus the conformational sampling on the lid region, positional restraints were applied to the MDM2 core domain (residues 30 to 119) (20 kcal mol^{-1} Å^{-2}) whereas residues 1 to 29 were allowed to evolve freely. Those restrictions were subsequently removed prior to the beginning of the US calculations.

Although aMD simulations were helpful to provide an enhanced sampling of lid conformations for WT-MDM2, pS17-MDM2 and S17D-MDM2 variants, the technique does not provide reliable information about the relative populations of the sampled conformations (Figure S1). To obtain equilibrium data (populations) from the biased aMD simulations, an Umbrella sampling calculation (US) is thus subsequently performed. Two collective variables were identified which could discriminate between several lid states: CV1 defines the extension of the lid as a function of the distance between the alpha carbons of residues 1 and 23 while CV2 is defined by the angle between the alpha carbons of residues 11, 50 and 62 (lid-core angle) (Figure 1). With these definitions the p53 binding site may be considered occluded by the MDM2 lid

when the lid-core angle is below 80º and the lid extension is larger than 24 Å. Other values would lead to an "open" state of the lid. US simulations were performed for WT,[24] pS17 and S17D variants. CV1 was sampled from 3 Å to 49 Å with a 2 Å interval and CV2 from 20º to 140º with a 6º interval. A total of 504 windows were thus defined. Each window used as a starting point the closest snapshot obtained during the preceding aMD simulations. aMD and US protocol example input files are provided in the SI (Dataset S1). A harmonic constraint of 1 kcal mol^{-1} $Å^{-2}$ and 0.12 kcal mol^{-1} deg^{-2} was used for CV1 and CV2 respectively. For each simulation bin, 500 ps simulation were performed to pre-equilibrate the system before accumulating statistics for 4 ns. Free energy profiles were obtained using the 2D variational Free Energy Profile (vFEP) method.[29,30] To estimate uncertainties in bin free energies, all US trajectories were sub-divided into four parts of equal duration and analysed separately (Fig. S2).

Analysis of the molecular dynamics trajectories

Trajectories and 3-D structures were visually inspected using Pymol[40] and VMD.[41] RMSDs, hydrogen bonds and hydrophobic lid/core contacts were monitored using cpptraj module in AmberTools12.[42] Average helical, sheet, turn or coil propensities were computed according to the DSSP code. [43,44] The formation of a hydrogen bond was considered when the distance between donor and acceptor was shorter or equal to 3.0 Å and the angle between the acceptor, hydrogen and donor atoms was equal or larger than 154°. A hydrophobic contact was defined when the distance between two carbon atoms was less than 5 Å. To avoid counting a large number of trivial contacts, for every lid residue *i*, intramolecular lid-lid hydrophobic contacts with immediate neighbouring residues (*i*+1, *i*-1) were excluded from the analysis.

All observables were obtained by reweighting statistics from the US snapshots according to equation 3.

$$< A_i > = \frac{\sum_{j=1}^{N}\left(\frac{1}{M}\sum_{k=1}^{M} A_{j,k}\right)\cdot e^{-\beta \Delta G_j}}{\sum_{J=1}^{N} e^{-\beta \Delta G_j}}, \quad (3)$$

where $<A_i>$ is the ensemble average of the property of interest for the lid residue i, N is the number of US bins, M is the number of snapshots in bin j, $A_{j,k}$ is the value of the property A_i for snapshot k in bin j and ΔG_j is the free energy of bin j obtained by vFEP reweighting. To estimate uncertainties in the computed properties, the simulation data was split in four consecutive blocks of 1 ns each and property values computed separately. Mean $<A_i>$ values are reported along with one standard error. For each system, representative lid structural ensembles were obtained by randomly selecting 10 snapshots from the pooled US snapshots according to their computed equilibrium probabilities. Representative snapshots are provided as PDB files in the SI (Dataset S2).

MMGBSA energy decomposition analysis

In addition to structural parameters derived from equation 1, estimates in the lid-core energetics were sought by means of MMGBSA analyses. Here the energetics of "binding" ($\Delta G_{binding}$) of the of the lid region (residues 1-24) to the core region (residues 30-100) was estimated via equation 4 as implemented in the software MMPBSA.py.[45]

$$\Delta G_{binding,solvated} = \Delta G_{core+lid,solvated} - \left[\Delta G_{core,solvated} + \Delta G_{lid,solvated}\right]. \quad (4)$$

The free energy change associated with each term on the right-hand side of equation 4 is given by equation 5:

$$\Delta G_{solvated} = E_{gas} + \Delta G_{solvation}. \quad (5)$$

where E_{gas} is the lid-core intermolecular gas phase energy, calculated using the AMBER force field (eq. 6).

$$E_{gas} = E_{elec} + E_{vdW}. \quad (6)$$

Bonded terms and intramolecular non-bonded energetics that are normally present in equation 6 were not included here as a 'single-trajectory' protocol was used and their contribution therefore cancel out.[46] The solvation free energy ($\Delta G_{solvation}$) is decomposed into polar and non-polar contributions (eq. 7).

$$\Delta G_{solvation} = \Delta G_{polar} + \Delta G_{non-polar}. \quad (7)$$

where polar contributions (ΔG_{polar}) to the solvation free energy are calculated by solving the generalized Born (GB) equation.[47] Non-polar terms were estimated from the nonpolar solvent accessible surface area (SASA).

$$\Delta G_{non-polar} = \gamma \text{SASA}, \quad (8)$$

where the surface tension constant γ has a value of 0.005 kcal mol^{-1} Å^{-2}. Other contributions to the binding energetics (such as solvent, or conformational entropies) are omitted in the present analysis. The calculated energies were then decomposed into per-lid residue contributions.[48,49]

The impact of Ser17 modifications on the MDM2 lid-core interaction energetics was determined by calculating the sum of polar interactions and the contribution of polar terms to the solvation free energy ($\Delta G_{elec,GB,i}$) and the sum of hydrophobic interactions and the contribution of non-polar groups to the solvation free energy ($\Delta G_{vdW,SA,i}$) for each lid residue *i*, minus the same the same values computed for WT-MDM2:

$$\Delta\Delta G_{elec,GB,i} = [\Delta G_{elec,GB,i}]^{S17*\text{-}MDM2} - [\Delta G_{elec,GB,i}]^{WT\text{-}MDM2}, \quad (9)$$

$$\Delta\Delta G_{vdW,SA,i} = [\Delta G_{vdW,SA,i}]^{S17*\text{-}MDM2} - [\Delta G_{vdW,SA,i}]^{WT\text{-}MDM2}, \quad (10)$$

where S17* refers to the modified Ser17 (pS17 or S17D).

Results

Influence of Ser17 phosphorylation and Ser17Asp mutation on the free energy landscape of the MDM2 lid

The free energy surfaces (FES) representing the conformational space occupied by the lid in pS17-MDM2 and S17D-MDM2 were compared to the FES previously obtained for the WT-MDM2 (Figure 2A).[24] WT-MDM2 displayed one "closed" conformation at CV1 = 31 Å, CV2 = 62º which corresponds to the lowest free energy region. Two local minima were located at CV1 = 10 Å, CV2 = 64º, and CV1= 7 Å, CV2 = 119º corresponding to a "semi-closed" and fully "open" states respectively.

The free energy surfaces (FES) obtained from US simulations of pS17-MDM2 showed one major low-free energy basin at CV1 = 27 Å; CV2 = 32º corresponding to a "closed" state of the lid and two additional local minima (CV1 = 12 Å; CV2 = 50º and CV1 = 20 Å; CV2 = 90º) that correspond to "semi-open" conformations 1 and 2 respectively (Figure 2B). However, fully "open" states were not detected in low free energy regions, in contrast to what was observed for WT-MDM2 (Figure 2A) where a fully accessible p53-binding pocket was present at CV1=7 Å, CV2=119º. The "closed" state in pS17-MDM2 also displays a semi-extended lid adopting a lower CV2 angle compared to the one observed for the WT-MDM2, as a result of a tighter interaction of the lid with helix α2 (Figure 2B). In this conformation, binding of the p53 TAD is hindered as a result of steric clashes with the lid, but nevertheless, the Phe19-Trp23-Leu26 cleft appears still accessible to small molecules such as Nutlins. The "semi-open" conformations were

similar to those detected in WT-MDM2: the lid adopts a semi-extended conformation approaching the core of MDM2, partially occluding the hydrophobic pocket of MDM2. Although this conformation would still limit the binding of p53, smaller MDM2 binders can access the binding site.

The FES of the phospho-mimetic S17D-MDM2 displayed a main free energy region at a "closed" conformation (CV1 = 29 Å; CV2= 56º) (Figure 2C). In this case, the lid-core angle is larger than the one observed for pS17 MDM2 and resembles more to the "closed" conformation of the WT-system. In this state, the hydrophobic cleft of MDM2 remains inaccessible to p53 TAD but, as was the case for WT-MDM2 and pSer17-MDM2, binding of small molecules is unlikely to be hindered. A second low free energy region corresponding to a "semi-open" conformation was detected in S17D-MDM2, in which the semi-extended configuration leads to a partially accessible hydrophobic pocket of MDM2. Interestingly, the lid was shown to be more extended compared to several "semi-open" conformations detected for pS17-MDM2 or WT-MDM2 (20 Å vs 10 Å). Finally, as for pS17-MDM2, no fully open conformations were detected for S17D-MDM2.

Impact of pSer17 and Ser17Asp modifications on MDM2 lid-core interactions.

The computed lid-core interactions of pS17-MDM2 and in S17D-MDM2 were inspected to provide a rationale for the different configurations observed in the FES. pSer17 in pSer17-MDM2 is frequently involved in hydrogen-bonding or electrostatic interactions (Figure 3A, left panel). Inspection of the conformational ensemble indicates that these arise predominantly in a 'closed' lid conformation that involves charge-charge interactions of pSer17 with residues His96 and Arg97. In addition, Tyr100 in helix α2', is frequently hydrogen-bonded to the pS17

backbone nitrogen (Figures 4A-B). In this closed lid conformation lid residue Ile19 is involved in significant non-polar (Figure 3A), and these contacts arise predominantly from packing with Tyr104. Finally, a backbone (NH)-backbone (CO) polar interaction is observed between Asn3 and Ans5 at the N-terminal end of the lid (Fig 3A, right panel).

The FES of pSer17-MDM2 contains a secondary low free energy region that was labelled "semi open state 1". In this conformation the lid is more compact, with its N-terminal end approaching C-terminal lid region (Figure 4C). In this state, pS17 still interacts with His96, but Arg97 is involved in a salt-bride with Asp23 at the C-terminal end of the lid. Three internal hydrogen bonds involving exclusively lid residues played an important role in the formation of the semi-extended conformation (Figure 3A right panel and Figure 4C). The Gln18 sidechain directly interacts with the phosphate from pS17, while Asp11 and Asn5 were hydrogen-bonded with Thr16 and Ileu19 respectively. The latter two residues also stabilize this conformation by establishing hydrophobic contacts with Met50 (Figure 3A left panel and Figure 4C).

The third low free energy region observed in the FES, "semi-open state 2", displayed a compact state of the lid. In this case, pSer17 preferentially interacted with Arg97 (Figure 4D). Here, most of the stabilizing interactions were shown to be hydrophobic. Particularly relevant were those involving Met6, Ileu19 and Pro20 that interacted with α2 helix residues Leu54 and Met50, partially occluding the accessibility to the p53-binding site (Figure 3A left panel, Figure 4D). In addition, stable lid-lid hydrophobic contacts are established between Val14 and Met6 while Met1 is in closed contact to Ala13 and Thr16 (Figure 3A right panel and Figure 4D).

Remarkably the patterns of lid-core interactions in S17D-MDM2 were significantly altered compared with pSer17-MDM2. In the closed state, the S17D residue remained largely solvent exposed and instead Asp11 forms salt-bridges with His96, and occasionally with Lys94

(Figure 3B, Left panel and Figure 5A-B). The interaction between Asp25 (first core residue following the lid) and Lys51 stabilises further the closed state. The lid adopts nevertheless a closed state owing to non-polar contacts formed by the N-terminal residues Met1, Cys2 and Met6 and the hydrophobic pocket residues Met62 and Val93.(Figure 3B and 5B). Val14 also favours this conformation by means of hydrophobic contacts with Met50, and Leu54 from helix α2. Visualisation of the conformational ensemble indicates that these lid residues frequently protrude deep into the p53 binding site (Figure 5B). Overall, lid-lid interactions were weaker compared with the pS17-MDM2 variant, with the exception of Met1-Met6 hydrophobic contacts (Figure 3B, right Panel). Finally, the semi-open conformation observed in S17D-MDM2 shows the lid interacting with α2 helix leaving the p53 binding pocket partially accessible. Such conformation mainly involves hydrophobic contacts between Met1/Pro9 and Phe55 (Figure 3B and 5C).

Impact of Ser17 phosphorylation and Ser17Asp mutation on MDM2 lid flexibility

Next the flexibility of the lid region was assessed via RMSD calculations. The overall lid flexibility in pS17-MDM2 and S17D-MDM2 (6.4±2.2 Å and 5.6±1.7 Å, respectively) was higher than what had been computed previously for WT-MDM2 (4.1±1.0 Å).[24] In WT-MDM2 significant hydrophobic contacts of the lid with helix α2 (e.g Ile19 and Ile20) contribute to a decrease in lid flexibility. By contrast in pS17-MDM2 and S17D-MDM2 the lid prefers to shift away from above helix α2 to occupy the p53 pocket where more space is available to accommodate conformational fluctuations.

Per-lid residue RMSD decomposition was used to gain finer insights into lid flexibility. In pSer17-MDM2 the most disordered residues were located at the N-terminal section of the lid. By contrast the C-terminal end close to the interface with the MDM2 core region was significantly more stable (Figure 6A). This is consistent with the previous observations indicating that the most important lid-core interactions in pS17-MDM2 involve residues pSer17 to Glu23. The least flexible residues are pSer17 and Ile19 due to their relatively higher number of polar and Van der Waals contacts with other core residues.

By contrast S17D-MDM2 shows broadly similar flexibility across N-terminal and C-terminal sections of the lid. This explains the overall decreased flexibility of the lid in this construct. The stabilisation of the N-terminal section can be traced to the network of non-polar contacts that Met6 forms in the p53 binding site. Residue Ser17Asp is as flexible as neighbouring residues since it is predominantly solvent-exposed.

Finally, the secondary structure propensities for every lid residue were computed for pS17-MDM2 and S17D-MDM2 (Fig. S3). While the non-phosphorylated lid displayed notable turn propensities near residues 8–13, 15–16 and 23–24 (Fig. S3A),[24] secondary structure elements were largely absent for the modified Ser systems.. The observed decreased propensity for adoption of secondary structure elements is in line with the increased flexibility displayed by the lid residues in pS17-MDM2 and S17D-MDM2.

Impact of Ser17 phosphorylation and Ser17Asp mutation on MDM2 lid-core interaction energetics

Next insights into lid-core energetics were sought. Overall estimates of relative free energies between open and close lid conformations were not computed owing to the difficulties of accurate evaluation of associated entropy changes.[22] Nevertheless insights can be gained in the

nature of the stabilising lid-core interactions by computing changes in residue interaction energies in pS17-MDM2 and S17D-MDM2 relative to WT-MDM2 (Figure 7). As expected, pS17 forms more favourable electrostatic interactions with the core with respect to unmodified Ser 17 ($\Delta\Delta G_{elec,GB}$ = -27.4 ± 2.1 kcal mol^{-1}) (Figure 7A). Contributions of Glu23 in pSer17-MDM2 and Asp11 in S17D-MDM2 were also more favourable compared with wild type MDM2 ($\Delta\Delta G_{elec,GB}$ = -5.6 ± 0.2 kcal mol^{-1} and -2.6 ± 0.9 kcal mol^{-1} respectively). On the other hand, non-polar terms contributions in pS17-MDM2 were moderately favoured or, most frequently, disfavoured (Figure 7B).

In S17D-MDM2 the contribution of polar lid residues are insignificant ($\Delta\Delta G_{elec,GB}$ for S17D = -0.4 ± 0.3 kcal mol^{-1}) (Figure 7A). The contribution of van der Waals interactions had as well a moderate effect on stabilizing the lid. Interestingly, the disfavoured non-polar contributions in the phospho-mimetic system corresponded to the lid residues located at the C-terminal end of the lid (notably Ile19 and Pro20: $\Delta\Delta G_{vdW,SA}$ = 5.8 ± 0.6 kcal mol^{-1} and $\Delta\Delta G_{vdW,SA}$ = 6.2 ± 0.2 kcal mol^{-1} respectively). On the contrary, van der Waals contributions were shown to be moderately favoured at the N-terminal end (Met6: $\Delta\Delta G_{vdW,SA}$ = -3.6 ± 0.1 kcal mol^{-1})

Discussion

Ser17 phosphorylation and Ser17Asp mutations stabilize closed conformations of the MDM2 lid

In comparison with WT-MDM2, the most remarkable difference observed in the free energy surfaces of pS17-MDM2 and S17D-MDM2 was the absence of low free energy fully "open" conformations. In both constructs “closed” and “semi-open” states are predominantly formed and they completely or partially occlude the p53-binding site (Figure 2).Thus the present

results support the work of McCoy et al.,[13] that suggested the S17D-MDM2 lid variant interacts more strongly with the MDM2 core region. The present results do not support the hypothesis of Worral et al. that the S17D mutation shifts the equilibrium towards an "open" lid state.[16,17] However such lid behaviour was inferred by Worral et al. from measured enhancements in the E3 ubiquitin ligase activity of S17D-MDM2 for p53. While the present results do not support the hypothesis that the MDM2 lid opens up upon phosphorylation, it remains possible that induced fit effects enable p53 to bind with phosphorylated MDM2, and that pSer17 or Ser17Asp plays a role in facilitating ubiquitination of p53 via MDM2. Indeed Zhan et al. have recently reported evidence that p53 may still bind to MDM2 independently of whether Ser17 is phosphorylated or mutated to its phospho-mimetic Ser17Asp.[15] Thus consideration of the impact of additional phosphorylation events on p53 TAD and/or MDM2 is desirable to clarify the role of these post-translational modifications on p53/MDM2 regulation.

The pSer17 and Ser17Asp lid structural ensembles differ significantly

Comparison of Figure 2A and 2B shows that the lowest free energy regions of the conformational ensemble of pS17-MDM2 occur at lower value of the CV2 angle than for WT-MDM2. This indicates that the lid region in pS17-MDM2 lies on average closer to the MDM2 α2 helix in the core region which implies a tighter interaction with the p53 binding site and helix α2. Contacts analyses and visualisation of the computed ensembles indicates that the phosphate group of pS17 is predominantly involved in salt-bridge interactions with His96 and Arg97 (Figures 3 and 4). These interactions, absent in WT lid,[24] stabilize further the lid in a closed state.

Comparison of Figure 2C and Figure 2A shows that Ser17Asp also destabilizes open lid states with respect to wild-type, but detailed structural analyses demonstrates that this occurs via a completely different pattern of lid-core interactions than with pSer17. The Ser17Asp residue remains largely solvent exposed, as was Ser17 in WT-MDM2. However, in WT-MDM2 open lid conformations bring Ser17 and Asp11 in close proximity. Bringing the negatively charged Asp17 in close proximity to the negatively charged Asp11 is energetically disfavoured in S17D-MDM2, as suggested by higher free energy value in open states (CV1 ca. 10 Å, CV2 ca. 110 degrees). In WT-MDM2 closed lid conformations Asp11 lies above the α2 helix, but in S17D-MDM2 this residue shifts position and predominantly forms salt-bridges with His96 and Lys94. This appears to 'drag' the rest of the N-terminal lid region from above the α2-helix to inside the p53 binding site, thus explaining the larger number of hydrophobic contacts of residues Met1 and Met6 with MDM2 core residues (Figure 3B). These findings are corroborated by the per-lid residue energy decomposition analysis that indicates phosphorylation of Ser17 introduces significantly favourable lid-core electrostatic interactions, whereas mutation of Ser17 into Asp17 has a smaller effect on interaction energetics (Figure 7).

The different patterns of observed lid-core interactions also result in significant variations in lid flexibility. Whereas the lid in pS17-MDM2 broadly decreases in flexibility from the N to C terminal sides, the lid in S17D-MDM2 exhibit similar flexibility across the N and C-terminal sides (Figure 6). With respect to wild type, enhanced interactions of pSer17 or Asp11 with Lys94 and His96 cause a shift away from the α2-helix, and concomitant loss of hydrophobic contacts. The result is an overall increase in lid flexibility.

Overall the picture that emerges is that both phosphorylation of Ser17 or mutation of Ser17 into Asp17 further stabilises closed lid states, but the conformational preferences and

flexibility of the closed lid states vary significantly. In order to mimic the structural and functional effects of protein phosphorylations, Ser/Thr mutations to Asp/Glu are frequently employed in biochemical experiments. However, in many cases the phospho-mimetic systems do not faithfully recapitulate the effect of protein phosphorylation,[50,51] due to important physicochemical differences between Glu or Asp and phosphorylated residues.[52] For instance, phosphorylated Ser/Thr display a tetrahedral topology and generally a -2 net charge, whereas Asp or Glu are planar and carry a net charge of -1. Moreover, the respective side chains are also dissimilar in size, the carbon atom having a smaller radius than phosphorus and the carboxylate group of the phospho-mimetic residues displaying two oxygen instead of three. Thus caution should be applied when interpreting the structural consequences of residue phosphorylation via phospho-mimetic analogues for this disordered protein region.

CONCLUSIONS

Molecular dynamics simulations support the hypothesis that phosphorylation of Ser17, or mutation of Ser17 into Asp17, both stabilise a closed conformational state of the MDM2 lid that is incompatible with binding of the p53 tumor suppressor. While both pS17-MDM2 and S17D-MDM2 variants were shown to significantly influence MDM2 lid behaviour, they do so through distinct molecular recognition mechanisms. In pS17-MDM2 the closed lid state is stabilized by salt-bridges between pSer17 and Lys94/His96, whereas in S17D-MDM2 it is Asp11 that predominantly interacts with Lys94/His96. The present results provide a clear rationale for the effect of Ser17 mutations on MDM2 lid-core interactions in unliganded MDM2. Further work is desirable to determine the consequences of phosphorylations on the stability of MDM2 bound to unphosphorylated and phosphorylated p53 peptide variants, and help formulate a fuller understanding of the role of post-translational modifications in p53 regulation.

Supporting Information

The Supporting Information is available free of charge on the ACS Publications website at DOI: XX.XXXX.

Dataset S1: Snapshots used to generate Figure 4 and Figure 5 (PDB format)

Dataset S2: Sample input files for the aMD and US simulations.

Table S1: aMD parameters used in the present simulations. All the parameters are given in $kcal.mol^{-1}$.

Figure S1: MDM2 lid distribution plot (in number of structures) projected on *x*: lid extension, in Å and *y*: lid-core angle, in degrees, obtained from aMD simulations. (A) WT-MDM2 simulations, adapted from Bueren-Calabuig et al.,[24] (B) pS17-MDM2, (C) S17D-MDM2.

Figure S2: Free energy surfaces for the MDM2 lid conformational changes projected on CV1 (lid extension, in Å) and CV2 (lid-core angle, in degrees) in different time windows. Energies are in $kcal.mol^{-1}$. (A) WT-MDM2 simulations, adapted from Bueren-Calabuig et al.,[24] (B) pS17-MDM2, (C) S17D-MDM2.

Figure S3. MDM2 lid secondary structure propensity. Red: helix; Green: Turn; Yellow: β-Strand. Black: Coil. Secondary structure definitions follow the DSSP code.[44] (A) WT-MDM2 simulations, adapted from Bueren-Calabuig et al.,[24] (B) pS17-MDM2, (C) S17D-MDM2.

References

(1) Brown, C. J., Lain, S., Verma, C. S., Fersht, A. R., and Lane, D. P. (2009) Awakening guardian angels: drugging the p53 pathway. *Nat. Rev. Cancer 9*, 862–873.

(2) Römer, L., Klein, C., Dehner, A., Kessler, H., and Buchner, J. (2006) p53—A Natural Cancer Killer: Structural Insights and Therapeutic Concepts. *Angew. Chem. Int. Ed. 45*, 6440–6460.

(3) Kussie, P. H., Gorina, S., Marechal, V., Elenbaas, B., Moreau, J., Levine, A. J., and Pavletich, N. P. (1996) Structure of the MDM2 oncoprotein bound to the p53 tumor suppressor transactivation domain. *Science 274*, 948–953.

(4) Oliner, J. D., Pietenpol, J. A., Thiagalingam, S., Gyuris, J., Kinzler, K. W., and Vogelstein, B. (1993) Oncoprotein MDM2 conceals the activation domain of tumour suppressor p53. *Nature 362*, 857–860.

(5) Li, J., and Kurokawa, M. (2015) Regulation of MDM2 Stability After DNA Damage. *J. Cell. Physiol. 230*, 2318–2327.

(6) Meek, D. W. (2015) Regulation of the p53 response and its relationship to cancer. *Biochem. J. 469*, 325–346.

(7) Meek, D. W., and Knippschild, U. (2003) Posttranslational modification of MDM2. *Mol. Cancer Res. 1*, 1017–1026.

(8) Michael, D., and Oren, M. (2003) The p53-Mdm2 module and the ubiquitin system. *Seminars in Cancer Biology 13*, 49–58.

(9) Appella, E., and Anderson, C. W. (2001) Post-translational modifications and activation of p53 by genotoxic stresses - Appella. *Eur. J. Biochem. 268*, 2764–2772.

(10) Brown, C. J., Cheok, C. F., Verma, C. S., and Lane, D. P. (2011) Reactivation of p53: from peptides to small molecules. *Trends Pharmacol. Sci. 32*, 53–62.

(11) Oliner, J. D., Kinzler, K. W., Meltzer, P. S., George, D. L., and Vogelstein, B. (1992) Amplification of a gene encoding a p53-associated protein in human sarcomas. *Nature 358*, 80–83.

(12) Mayo, L. D., Turchi, J. J., and Berberich, S. J. (1997) Mdm-2 phosphorylation by DNA-dependent protein kinase prevents interaction with p53. *Cancer research 57*, 5013–5016.

(13) McCoy, M. A., Gesell, J. J., Senior, M. M., and Wyss, D. F. (2003) Flexible lid to the p53-binding domain of human Mdm2: Implications for p53 regulation. *Proc. Natl. Acad. Sci. U.S.A.*

100, 1645–1648.
(14) Fraser, J. A., Worrall, E. G., Lin, Y., Landre, V., Pettersson, S., Blackburn, E., Walkinshaw, M., Muller, P., Vojtesek, B., Ball, K., and Hupp, T. R. (2015) Phosphomimetic mutation of the N-terminal lid of MDM2 enhances the polyubiquitination of p53 through stimulation of E2-ubiquitin thioester hydrolysis. *J. Mol. Biol. 427*, 1728–1747.
(15) Zhan, C., Varney, K., Yuan, W., Zhao, L., and Lu, W. (2012) Interrogation of MDM2 Phosphorylation in p53 Activation Using Native Chemical Ligation: The Functional Role of Ser17 Phosphorylation in MDM2 Reexamined. *J. Am. Chem. Soc. 134*, 6855–6864.
(16) Worrall, E. G., Worrall, L., and Blackburn, E. (2010) The Effects of Phosphomimetic Lid Mutation on the Thermostability of the N-terminal Domain of MDM2. *J. Mol. Biol. 398*, 414–428.
(17) Worrall, E. G., Wawrzynow, B., Worrall, L., Walkinshaw, M., Ball, K. L., and Hupp, T. R. (2009) Regulation of the E3 ubiquitin ligase activity of MDM2 by an N-terminal pseudo-substrate motif. *J. Chem. Biol. 2*, 113–129.
(18) Pantelopulos, G. A., Mukherjee, S., and Voelz, V. A. (2015) Microsecond simulations of mdm2 and its complex with p53 yield insight into force field accuracy and conformational dynamics. *Proteins. 83*, 1665–1676.
(19) Verkhivker, G. M. (2012) Simulating Molecular Mechanisms of the MDM2-Mediated Regulatory Interactions: A Conformational Selection Model of the MDM2 Lid Dynamics. *PLoS ONE 7*, e40897.
(20) Dastidar, S. G., Raghunathan, D., Nicholson, J., Hupp, T. R., Lane, D. P., and Verma, C. S. (2011) Chemical states of the N-terminal "lid" of MDM2 regulate p53 binding: Simulations reveal complexities of modulation. *Cell Cycle 10*, 82–89.
(21) Showalter, S. A., Bruschweiler-Li, L., Johnson, E., Zhang, F., and Brüschweiler, R. (2008) Quantitative Lid Dynamics of MDM2 Reveals Differential Ligand Binding Modes of the p53-Binding Cleft. *J. Am. Chem. Soc. 130*, 6472–6478.
(22) Michel, J. (2014) Current and emerging opportunities for molecular simulations in structure-based drug design. *Phys. Chem. Chem. Phys. 16*, 4465–4477.
(23) Cuchillo, R., and Michel, J. (2012) Mechanisms of small-molecule binding to intrinsically disordered proteins. *Biochem. Soc. Trans. 40*, 1004–1008.
(24) Bueren-Calabuig, J. A., and Michel, J. (2015) Elucidation of Ligand-Dependent Modulation

of Disorder-Order Transitions in the Oncoprotein MDM2. *PLoS Comput. Biol. 11*, e1004282.
(25) Pierce, L. C. T., Salomon-Ferrer, R., Augusto F de Oliveira, C., McCammon, J. A., and Walker, R. C. (2012) Routine Access to Millisecond Time Scale Events with Accelerated Molecular Dynamics. *J. Chem. Theory Comput. 114*, 2997–3002.
(26) Markwick, P. R. L., and McCammon, J. A. (2011) Studying functional dynamics in bio-molecules using accelerated molecular dynamics. *Phys. Chem. Chem. Phys. 13*, 20053–20065.
(27) Hamelberg, D., Mongan, J., and McCammon, J. A. (2004) Accelerated molecular dynamics: a promising and efficient simulation method for biomolecules. *J. Chem. Phys. 120*, 11919–11929.
(28) Torrie, G. M., and Valleau, J. P. (1977) Nonphysical sampling distributions in Monte Carlo free-energy estimation: Umbrella sampling. *J. Comput. Phys 23*, 187–199.
(29) Lee, T. S., Radak, B. K., Huang, M., Wong, K.-Y., and York, D. M. (2014) Roadmaps through Free Energy Landscapes Calculated Using the Multidimensional vFEP Approach. *J. Chem. Theory Comput. 10*, 24–34.
(30) Lee, T. S., Radak, B. K., Pabis, A., and York, D. M. (2013) A New Maximum Likelihood Approach for Free Energy Profile Construction from Molecular Simulations. *J. Chem. Theory Comput. 9*, 153–164.
(31) Uhrinova, S., Uhrin, D., Powers, H., Watt, K., Zheleva, D., Fischer, P., McInnes, C., and Barlow, P. N. (2005) Structure of free MDM2 N-terminal domain reveals conformational adjustments that accompany p53-binding. *J. Mol. Biol. 350*, 587–598.
(32) Case, D. A., Darden, T. A., Cheatham, T. E. 3., Simmerling, C., Wang, J., Duke, R. E., Luo, R., Walker, R. C., Zhang, W., Merz, K. M., S, R., Hayik, A., Roitberg, A. E., de M Seabra, G., Swails, J., Goetz, A. W., Kolossvary, I., Wong, K. F., Paesani, F., Vanicek, J., Wolf, R. M., Liu, J., Wu, X., Brozell, S. R., Steinbrecher, T., Gohlke, H., Cai, Q., Ye, X., Hsieh, J., Cui, G., Roe, D. R., Mathews, D. H., Seeting, M. G., Salomon-Ferrer, R., Sagui, C., Babin, V., Luchko, T., Gusarov, S., Kovalenko, A., and Kollman, P. A. (2012) AMBER12. *Amber 12; University of California, San Francisco*.
(33) Li, D.-W., and Brüschweiler, R. (2010) NMR-Based Protein Potentials. *Angew. Chem. Int. Ed. 122*, 6930–6932.
(34) Homeyer, N., Horn, A. H. C., Lanig, H., and Sticht, H. (2006) AMBER force-field parameters for phosphorylated amino acids in different protonation states: phosphoserine,

phosphothreonine, phosphotyrosine, and phosphohistidine. *J. Mol. Model. 12*, 281–289.
(35) Jorgensen, W. L., Chandrasekhar, J., Madura, J. D., Impey, R. W., and Klein, M. L. (1983) Comparison of simple potential functions for simulating liquid water. *J. Chem. Phys. 79*, 926–935.
(36) Aaqvist, J. (1990) Ion-water interaction potentials derived from free energy perturbation simulations. *J. Phys. Chem. B 94*, 8021–8024.
(37) Iannuzzi, M., Laio, A., and Parrinello, M. (2003) Efficient Exploration of Reactive Potential Energy Surfaces Using Car-Parrinello Molecular Dynamics. *Phys. Rev. Lett. 90*, 238302.
(38) Laio, A., and Parrinello, M. (2002) Escaping free-energy minima. *Proc. Natl. Acad. Sci. U.S.A. 99*, 12562–12566.
(39) Bucher, D., Grant, B. J., Markwick, P. R., and McCammon, J. A. (2011) Accessing a hidden conformation of the maltose binding protein using accelerated molecular dynamics. *PLoS Comput. Biol. 7*, e1002034.
(40) Delano, W. L. (2002) The PyMOL Molecular Graphics System. *The PyMOL Molecular Graphics System. Schrödinger*.
(41) Humphrey, W., Dalke, A., and Schulten, K. (1996) VMD: Visual molecular dynamics. *J Mol Graphics 14*, 33–38.
(42) Roe, D. R., and Cheatham, T. E., III. (2013) PTRAJ and CPPTRAJ: Software for Processing and Analysis of Molecular Dynamics Trajectory Data. *J. Chem. Theory Comput. 9*, 3084–3095.
(43) Joosten, R. P., Beek, te, T. A. H., Krieger, E., Hekkelman, M. L., Hooft, R. W. W., Schneider, R., Sander, C., and Vriend, G. (2011) A series of PDB related databases for everyday needs. *Nucleic Acids Res. 39*, D411–9.
(44) Kabsch, W., and Sander, C. (1983) Dictionary of protein secondary structure: Pattern recognition of hydrogen-bonded and geometrical features - Kabsch - 2004 - Biopolymers - Wiley Online Library. *Biopolymers 22*, 2577–2637.
(45) Miller, B. R., III, McGee, T. D., Jr., Swails, J. M., Homeyer, N., Gohlke, H., and Roitberg, A. E. (2012) MMPBSA.py: An Efficient Program for End-State Free Energy Calculations. *J. Chem. Theory Comput. 8*, 3314–3321.
(46) Hou, T., Wang, J., Li, Y., and Wang, W. (2011) Assessing the performance of the MM/PBSA and MM/GBSA methods. 1. The accuracy of binding free energy calculations based on molecular dynamics simulations. *J. Chem. Inf. Model. 51*, 69–82.

(47) Onufriev, A., Bashford, D., and Case, D. A. (2000) Modification of the Generalized Born Model Suitable for Macromolecules. *J. Phys. Chem. B 104*, 3712–3720.
(48) Metz, A., Pfleger, C., Kopitz, H., Pfeiffer-Marek, S., Baringhaus, K.-H., and Gohlke, H. (2011) Hot Spots and Transient Pockets: Predicting the Determinants of Small-Molecule Binding to a Protein–Protein Interface. *J. Chem. Inf. Model. 52*, 120–133.
(49) Gohlke, H., Kiel, C., and Case, D. A. (2003) Insights into protein-protein binding by binding free energy calculation and free energy decomposition for the Ras-Raf and Ras-RalGDS complexes. *J. Mol. Biol. 330*, 891–913.
(50) Groban, E. S., Narayanan, A., and Jacobson, M. P. (2006) Conformational changes in protein loops and helices induced by post-translational phosphorylation. *PLoS Comput. Biol. 2*, e32.
(51) Zheng, W., Zhang, Z., Ganguly, S., Weller, J. L., Klein, D. C., and Cole, P. A. (2003) Cellular stabilization of the melatonin rhythm enzyme induced by nonhydrolyzable phosphonate incorporation. *Nat. Struct. Biol. 10*, 1054–1057.
(52) Tarrant, M. K., and Cole, P. A. (2009) The chemical biology of protein phosphorylation. *Annu. Rev. Biochem. 78*, 797–825.

Figure Legends

Figure 1. N-terminal domain of apo-MDM2 (residues 1–119) displaying the "open" and "closed" conformations. The lid (residues 1-24) is shown in green, the core (25-119) is displayed in blue. (A) The lid adopts an "open" conformation in the presence of the p53 transactivation domain (TAD) (in magenta). p53 residues Phe19, Trp23 and Leu26 protruding into the MDM2 hydrophobic pocket are shown in sticks. (B) MDM2 lid "closed" conformation competing with p53 for its binding site in the MDM2 core.

Figure 2. Free energy landscapes of wild type and modified Ser17-MDM2 lid. CV1 (lid extension) in Å and CV2 (lid-core angle) in degrees. Free energy contours (kcal mol^{-1}) are shown as a colour coded heat map. For every system, representative structures of MDM2 displaying 10 lid conformations from the global and local minima are shown. Ser17 is represented in red sticks. (A) WT-MDM2, adapted from Bueren-Calabuig et al.[24] (B) pS17-MDM2 (C) S17D-MDM2

Figure 3. MDM2 lid intermolecular and intramolecular interactions in pS17-MDM2 and S17D-MDM2. Lid-core and lid-lid hydrophobic contacts are shown in red and maroon respectively; core and lid-lid hydrogen bonds are displayed in blue and green respectively. (A) pS17-MDM2 (B) S17D-MDM2. Left) lid-core intermolecular interactions. Right) lid-lid intramolecular interactions.

Figure 4. MDM2 lid structural ensemble for pS17-MDM2. Structural ensemble (A) and structural details of the closed (B) and semi open states 1 (C) and 2 (D).

Figure 5. MDM2 lid structural ensemble for S17D-MDM2. Structural ensemble (A) and structural details of the closed (B) and semi open states (C).

Figure 6. MDM2 lid flexibility. Per residue average RMSD in pS17-MDM2 (A) and S17D-MDM2 (B).

Figure 7. Impact of Ser17 modification on lid-core binding energetics. (A) Decomposition of the contribution of the polar interaction energies to the total binding free energy for the pS17 MDM2 (black) and S17D (grey): $\Delta\Delta G_{elec,GB}=[\Delta G_{elec,GB}]^{S17*\text{-}MDM2} - [\Delta G_{elec,GB}]^{WT\text{-}MDM2}$ (B) Decomposition of the contribution of the non polar interaction energies to the total binding free energy for the pS17 MDM2 (black) and S17D (grey): $\Delta\Delta G_{vdW,SA}=[\Delta G_{vdW,SA}]^{S17*\text{-}MDM2} - [\Delta G_{vdW,SA}]^{WT\text{-}MDM2}$ S17* represents pS17 or S17D.

Figure 1

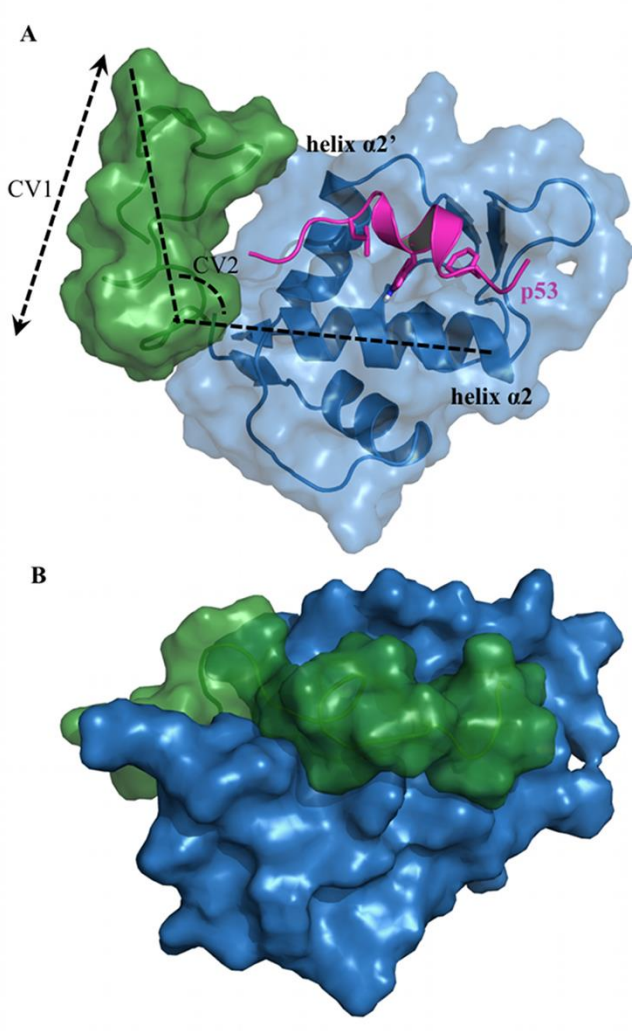

Figure 2

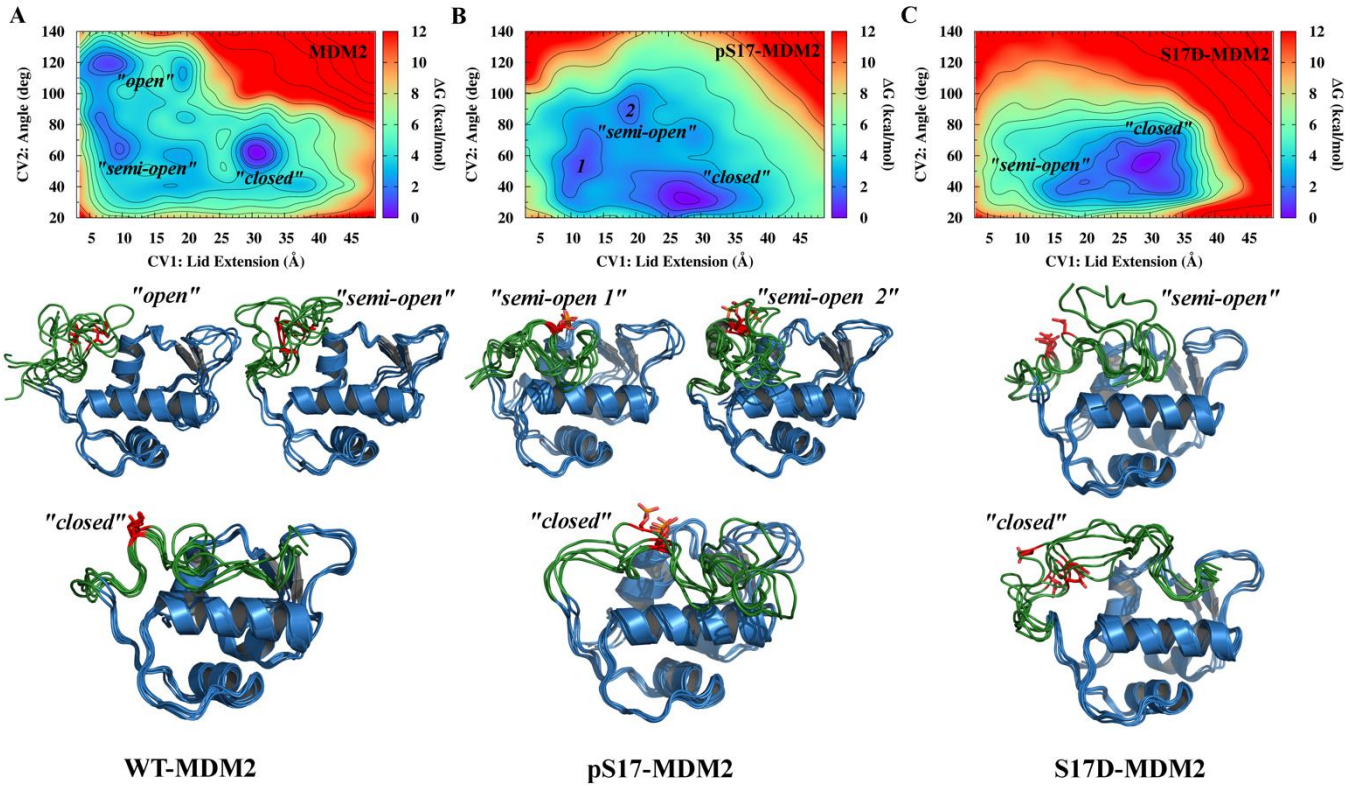
A
B
C
MDM2
pS17-MDM2
S17D-MDM2
"open"
"semi-open"
"closed"
"semi-open 1"
"semi-open 2"
1
2
CV2: Angle (deg)
CV1: Lid Extension (Å)
ΔG (kcal/mol)
WT-MDM2
pS17-MDM2
S17D-MDM2

Figure 3

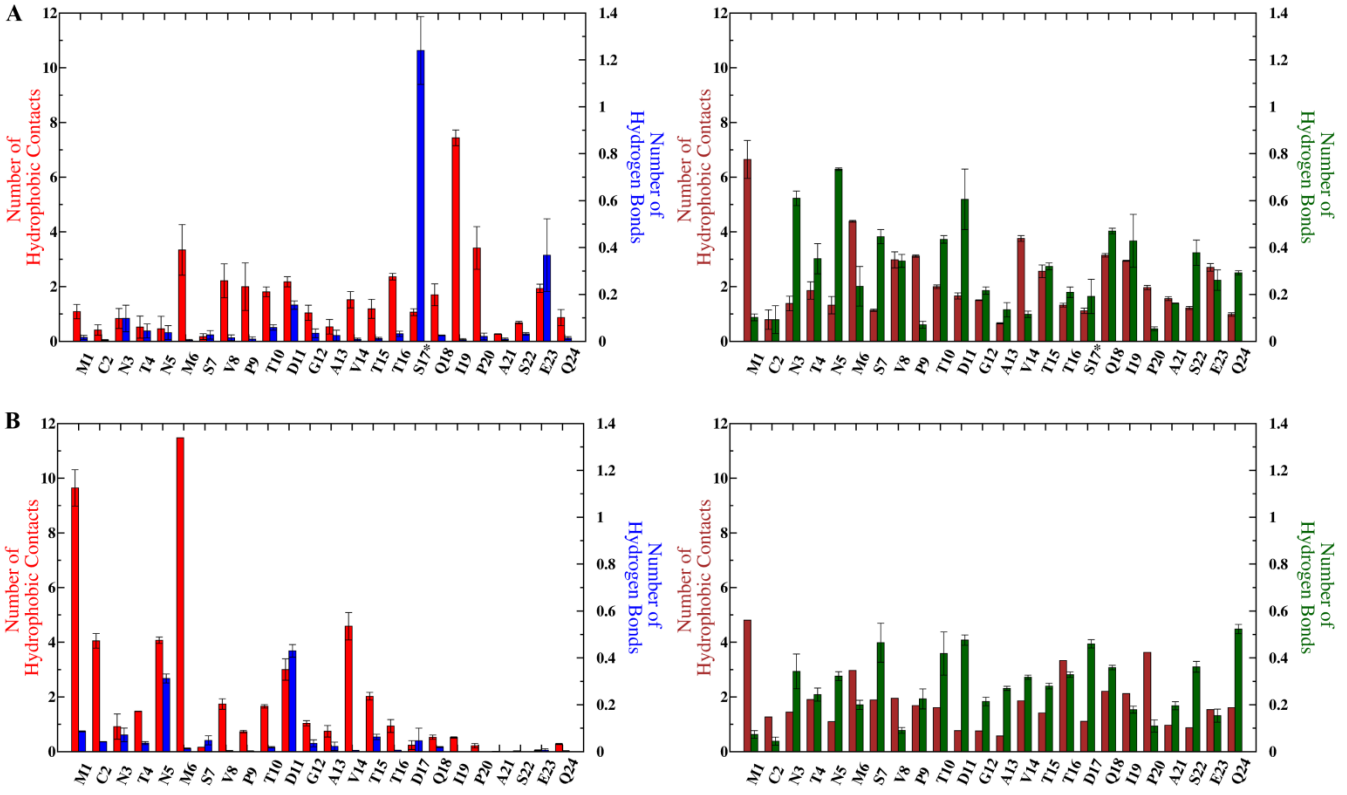
A
B
Number of Hydrophobic Contacts
Number of Hydrogen Bonds
M1 C2 N3 T4 N5 M6 S7 V8 P9 T10 D11 G12 A13 V14 T15 T16 S17* Q18 I19 P20 A21 S22 E23 Q24
M1 C2 N3 T4 N5 M6 S7 V8 P9 T10 D11 G12 A13 V14 T15 T16 S17* Q18 I19 P20 A21 S22 E23 Q24
M1 C2 N3 T4 N5 M6 S7 V8 P9 T10 D11 G12 A13 V14 T15 T16 D17 Q18 I19 P20 A21 S22 E23 Q24
M1 C2 N3 T4 N5 M6 S7 V8 P9 T10 D11 G12 A13 V14 T15 T16 D17 Q18 I19 P20 A21 S22 E23 Q24

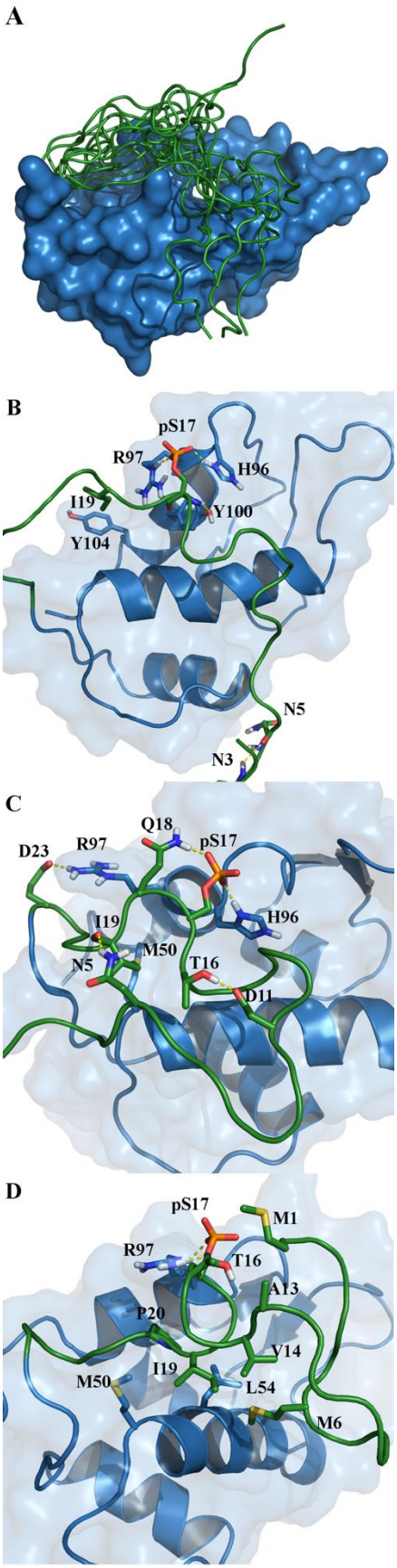
A
B
pS17
R97
H96
I19
Y100
Y104
N5
N3
C
Q18
D23
R97
pS17
H96
I19
M50
N5
T16
D11
D
pS17
M1
R97
T16
A13
P20
V14
I19
M50
L54
M6

Figure 4.

Figure 5

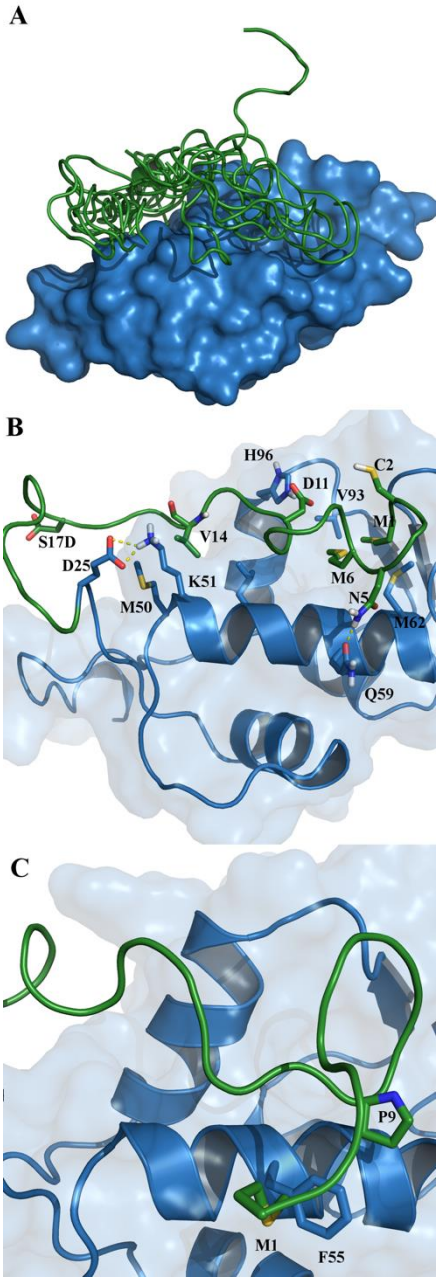

Figure 6

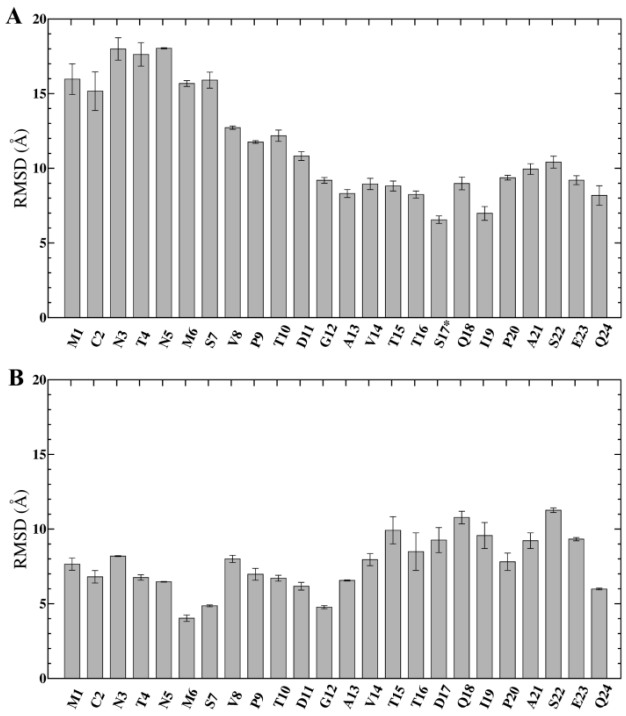
A
RMSD (Å)
0
5
10
15
20
M1 C2 N3 T4 N5 M6 S7 V8 P9 T10 D11 G12 A13 V14 T15 T16 S17* Q18 I19 P20 A21 S22 E23 Q24
B
RMSD (Å)
0
5
10
15
20
M1 C2 N3 T4 N5 M6 S7 V8 P9 T10 D11 G12 A13 V14 T15 T16 D17 Q18 I19 P20 A21 S22 E23 Q24

Figure 7

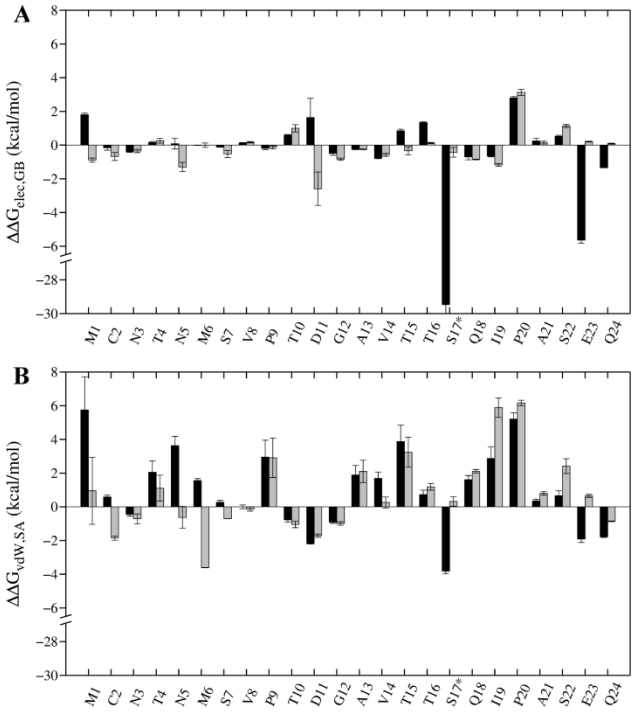
A
B
$\Delta\Delta G_{elec,GB}$ (kcal/mol)
$\Delta\Delta G_{vdW,SA}$ (kcal/mol)
8
6
4
2
0
−2
−4
−6
−28
−30
M1
C2
N3
T4
N5
M6
S7
V8
P9
T10
D11
G12
A13
V14
T15
T16
S17*
Q18
I19
P20
A21
S22
E23
Q24

For Table of Contents Use Only

"Impact of Ser17 phosphorylation on the conformational dynamics of the oncoprotein MDM2"

Juan A. Bueren-Calabuig and Julien Michel